Supporting Information

Tightly intercalated $Ti_3C_2T_x$/MoO_{3-x}/PEDOT:PSS free-standing films with high volumetric/gravimetric performance for flexible solid-state supercapacitors

Pengxue Zhang[a], Yan Sui[a], Weijing Ma[a], Nannan Duan[a], Qi Liu[a], Bingmiao Zhang[a], Haijun Niu[a,b], Chuanli Qin[a,b*]

[a] School of Chemistry and Material Science, Heilongjiang University, Harbin, 150080, China.

[b] Key Laboratory of Chemical Engineering Process & Technology for High-efficiency Conversion, College of Heilongjiang Province, Harbin, 150080, China.

[*] Email: qinchuanli@hlju.edu.cn. Tel: +86-0451-8660-8543.

Materials and Methods

Synthesis of MoO_{3-x} Nanobelts

0.24 g molybdenum powder was slowly added to 5 mL of 30% H_2O_2 and stirred for 10 min in an ice-water bath. After it was cooled to room temperature, 25 mL of deionized water and 5 mL of anhydrous ethanol were added, stirred until the solution turned yellow and then transferred to a stainless steel reactor for 18 h at 120 °C. Finally, MoO_{3-x} nanobelts were washed repeatedly with distilled water and ethanol, then dried in a vacuum oven at 60 °C for 12 h.

Synthesis of $Ti_3C_2T_x$ dispersion

1.0 g LiF and 20 mL of 9 M HCl aqueous solution were stirred for 10 min in an ice-water bath, and then 1.0 g Ti_3AlC_2 was slowly added to the above solution and stirred at 35 °C for 24 h. After the suspension was centrifuged at 3500 rmp for 5 min, the supernatant was decanted and washed with deionized water. The centrifugation process was repeated until pH of the supernatant was about 6. Finally, the precipitate was re-dispersed in deionized water and further sonicated for 1 h. After centrifuging at 3500 rpm for 1 h, the supernatant was taken as the $Ti_3C_2T_x$ dispersions (1.5 mg mL^{-1}).

Synthesis of $Ti_3C_2T_x/MoO_{3-x}$/PEDOT:PSS free-standing films

A certain amount of 1 mg mL^{-1} MoO_{3-x} aqueous suspension and 100 μL of 1.5 wt % PEDOT:PSS aqueous solution were added to 10 mL of 1.5 mg mL^{-1} $Ti_3C_2T_x$ dispersions by sonication for 30 min and stirred for 2 h. The free-standing films were obtained by vacuum filtration of the mixed suspension using PTFE membrane. At last, $Ti_3C_2T_x/MoO_{3-x}$/PEDOT:PSS free-standing films were obtained by soaking in 18 M H_2SO_4 solution for 24 h, washing with deionized water for several times and drying in the oven for 8 h at 60 °C to remove PSS. The $Ti_3C_2T_x/MoO_{3-x}$/PEDOT:PSS free-standing films with different amounts of MoO_{3-x} were named as TMP-1, TMP-2 and TMP-3, respectively. By comparison, $Ti_3C_2T_x$, $Ti_3C_2T_x/MoO_{3-x}$ and $Ti_3C_2T_x$/PEDOT:PSS free-standing films were also synthesized with the same process. The detailed experimental parameters can be found in Table S1. Meanwhile, the $Ti_3C_2T_x/MoO_{3-x}$/PEDOT:PSS free-standing films without H_2SO_4 soaking were also

obtained, which are named as TMP-U-1, TMP-U-2 and TMP-U-3, respectively.

Preparation of electrodes

2 mg of free-standing film was put between two pieces of stainless steel mesh, which is used as the collector in our work, and then pressed with the tablet press machine to obtain the electrode.

Preparation of flexible solid-state symmetrical supercapacitors

First, the PVA-H_2SO_4 gel electrolyte is prepared. 3.0 g PVA and 30 mL of 1M H_2SO_4 aqueous solution were stirred at 90 °C for 30 minutes until the solution became homogeneous and clear. Next, the resulting solution was cast into a mold and cooled to room temperature, followed by a freeze-thaw process (-20°C for 8 hours and thawed at room temperature for 3 hours, three times) to form the PVA-H_2SO_4 gel electrolyte. After that, the gel electrolyte was placed between two identical electrodes to assemble a flexible solid-state supercapacitor, which was sealed with the hot-melt adhesives after wrapped with PET film.

Characterization

Scanning electron microscopy (SEM, Zeiss, Gemini SEM 300, Germany) and transmission electron microscopy (TEM, Hitachi, H7650, Japan) were used to study the morphology and microstructure of samples. X-ray diffraction (XRD, Bruker, D8 ADV ANCE, Germany) analysis was performed to study the phase structure using Cu Kα radiation at 40 kV and 30 mA. Fourier transform infrared (FTIR) spectra were collected using detected with a Bruker Equiox 55 spectrometer, using the KBr pellet technique. X-ray photoelectron spectroscopy (XPS) experiments were performed using an ESCALAB 250 electron spectrometer (Thermo Fisher Scientific, USA) to confirm the composition and elemental chemical state on the surface of samples. A remote computer-controlled contact angle goniometer system (Dataphysics oca-20, Germany) was used to examine the surface wettability of samples.

Electrochemical measurements

In the three-electrode system, the prepared electrodes were used as working electrodes, and Ag/AgCl and platinum foils were used as reference and counter electrodes, respectively. Cyclic voltammetry (CV) tests were performed by a

computerized electrical analysis system (Tianjin Lannico, LK98B II, China) in the potential window range of -0.4 to 0.3 V. An electrochemical workstation (Shanghai Chenhua, CHI660E, China) was used for charge/discharge (GCD) measurements with the same potential window at constant currents. Electrochemical impedance spectroscopy (EIS) measurements were performed over a frequency range of 0.01 Hz to 100 kHz with an amplitude of 10 mV-0.1 V at open-circuit potentials of -0.1 V with the same electrochemical workstation as the GCD measurements. All three-electrode measurements were performed at room temperature in 1 M H_2SO_4 aqueous solution.

The density (ρ) of free-standing films is calculated according to equation (S1).

$$\rho=\frac{m}{s\times d} \tag{S1}$$

where m (g), s (cm^2) and d (cm) are the mass, area and thickness of free-standing films, respectively.

The specific capacitance of film electrode materials can be calculated from the GCD curve using the following equations.

$$C_{g,1}=\frac{I\times\Delta t}{m\times\Delta V} \tag{S2}$$

$$C_{v,1}=\rho\times C_{g,1} \tag{S3}$$

where $C_{g,1}$ ($F\ g^{-1}$) and $C_{v,1}$ ($F\ cm^{-3}$) are the volumetric capacitance and gravimetric capacitance of film electrode materials, respectively, I(A) is the applied current, Δt(s) is the discharge time, m(g) is the mass of film electrode materials, and ΔV(V) is the potential range after the IR drop.

In the two-electrode system, GCD and CV measurements were performed using a battery test system (Landian, CT2001A, China) and a computerized electrical analysis system LK98B II, respectively. The specific capacitance, power density and energy density of symmetrical supercapacitors were calculated from the GCD curves according to the following equations.

$$C_{g,2}=\frac{I\times\Delta t}{m\times\Delta V} \tag{S4}$$

$$C_{v,2}=\rho\times C_{g,2} \tag{S5}$$

$$E_{g,2}=\frac{C_{g,2}\times\Delta V^2}{7.2} \tag{S6}$$

$$P_{g,2}=\frac{3600\times E_{g,2}}{\Delta t} \quad \text{(S7)}$$

$$E_{v,2}=\frac{C_{v,2}\times \Delta V^2}{7.2} \quad \text{(S8)}$$

$$P_{v,2}=\frac{3600\times E_{v,2}}{\Delta t} \quad \text{(S9)}$$

where $C_{g,2}$ (F g^{-1}) and $C_{v,2}$ (F cm^{-3}) are the volumetric and gravimetric capacitances of supercapacitors, respectively; I (A) is the applied current; Δt (s) is the discharge time; m (g) is the mass of film electrode materials on the two electrodes; ΔV (V) is the potential range after IR drop; ρ is the density of film electrode materials (g cm^{-3}); $P_{g,2}$ (W kg^{-1}) is the gravimetric power density; $E_{g,2}$ is the gravimetric energy density (Wh kg^{-1}); $P_{v,2}$ is the volumetric power density (W L^{-1}); $E_{v,2}$ is the volumetric energy density (Wh L^{-1})

Results and discussion

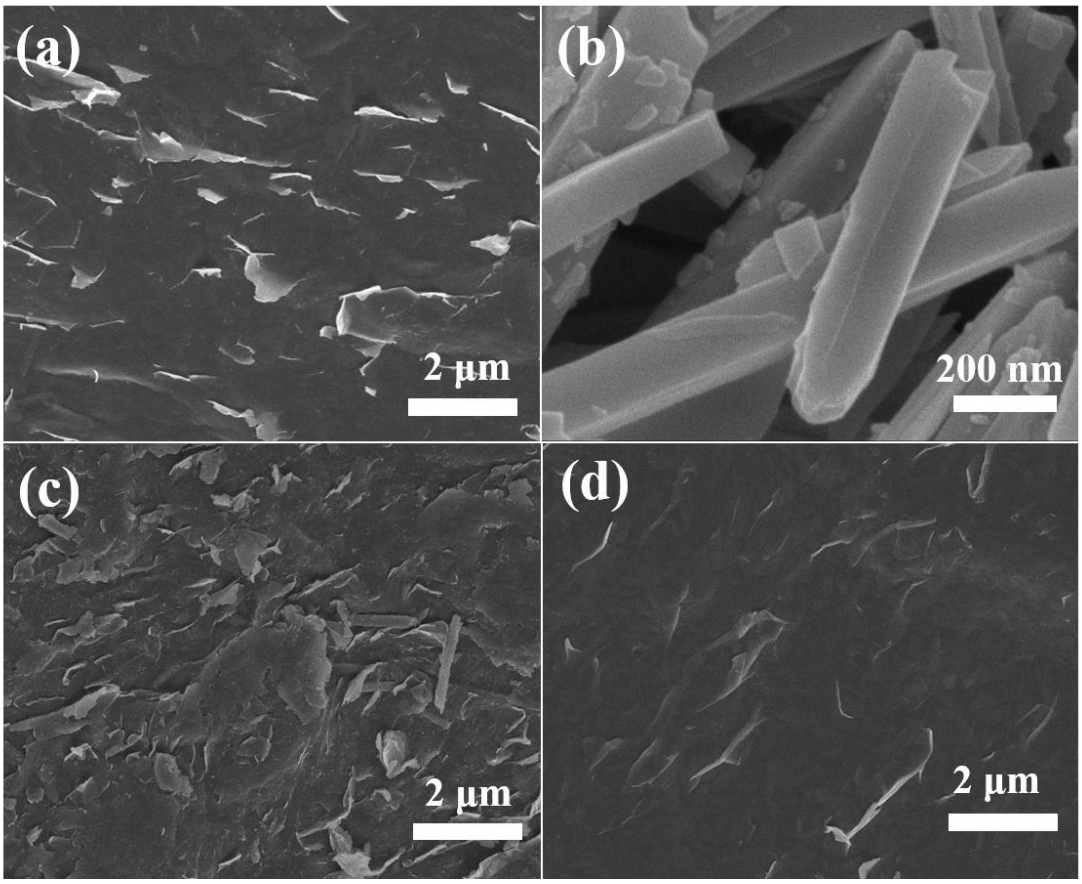

Fig.S1. SEM images of (a) $Ti_3C_2T_x$; (b) MoO_{3-x}; (c) $Ti_3C_2T_x/MoO_{3-x}$; (d) $Ti_3C_2T_x$/PEDOT:PSS.

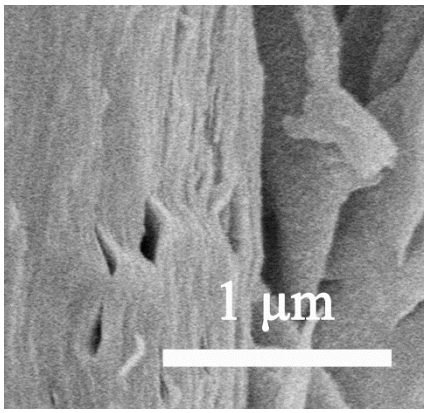

Fig.S2. Cross-sectional SEM image of $Ti_3C_2T_x$.

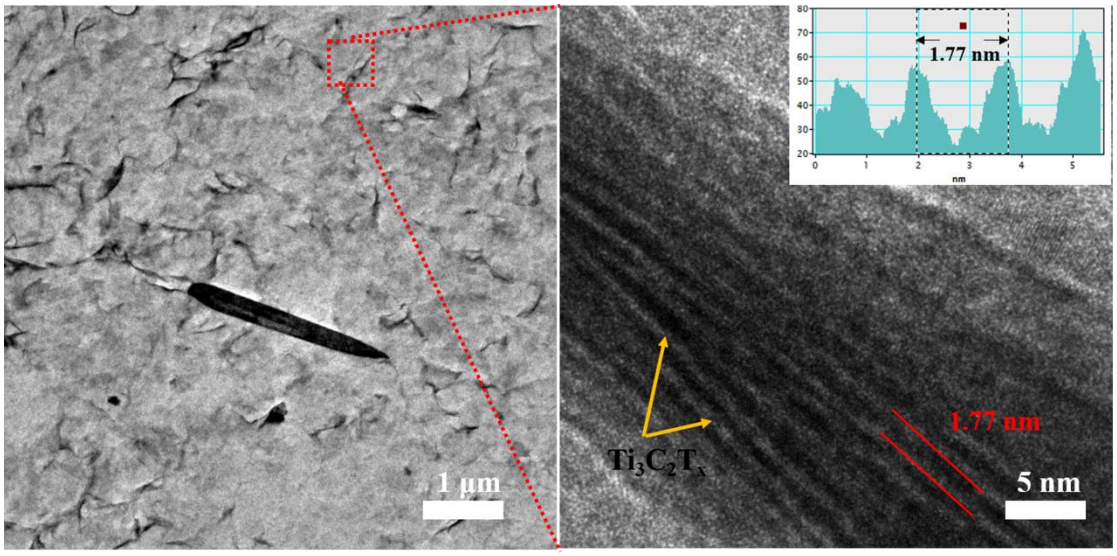

Fig.S3. (a) TEM and (b) HRTEM images of TMP-2.

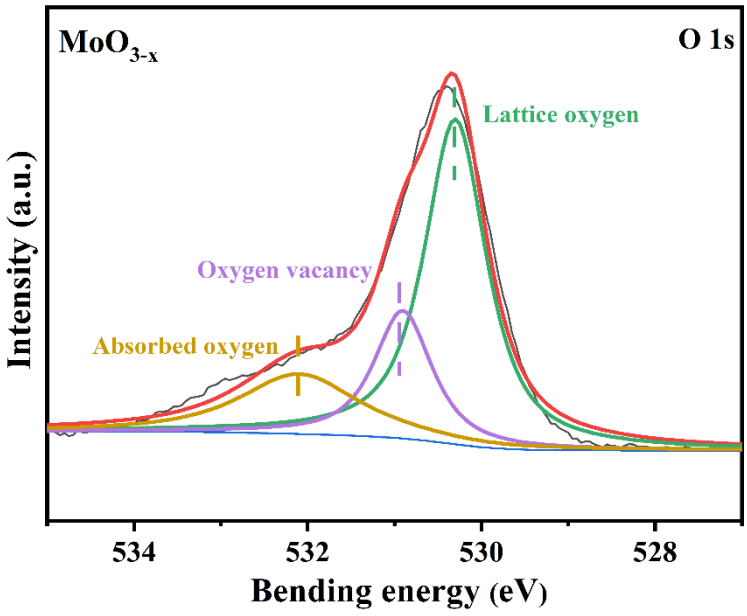

Fig.S4. High resolution O1s XPS spectra of MoO_{3-x}.

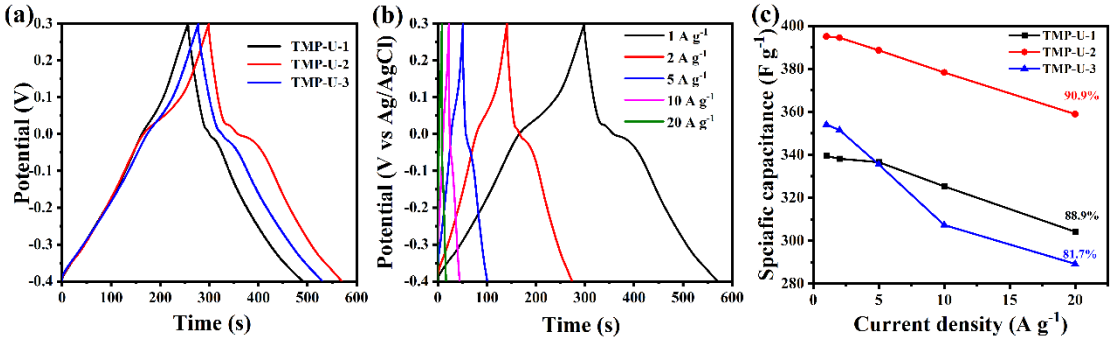

Fig.S5. GCD curves of (a) different samples at 1 A g^{-1} and (b) TMP-U-2 at different current densities; (c) Gravimetric capacitance of the as-prepared film electrodes as a function of current density.

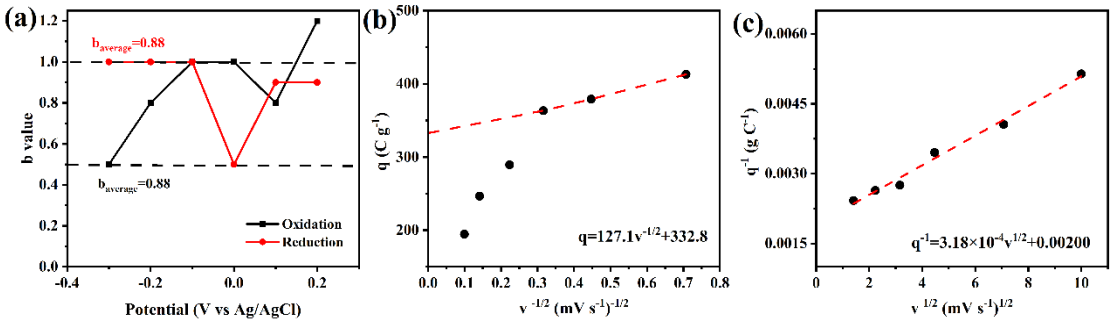

Fig.S6. (a) Calculated *b* value of TMP-2 for the oxidized and reduced portions vs potential; Dependence of (b) *q* on $v^{-1/2}$ and (c) q^{-1}on $v^{1/2}$ for TMP-2 electrodes in 1 M H_2SO_4.

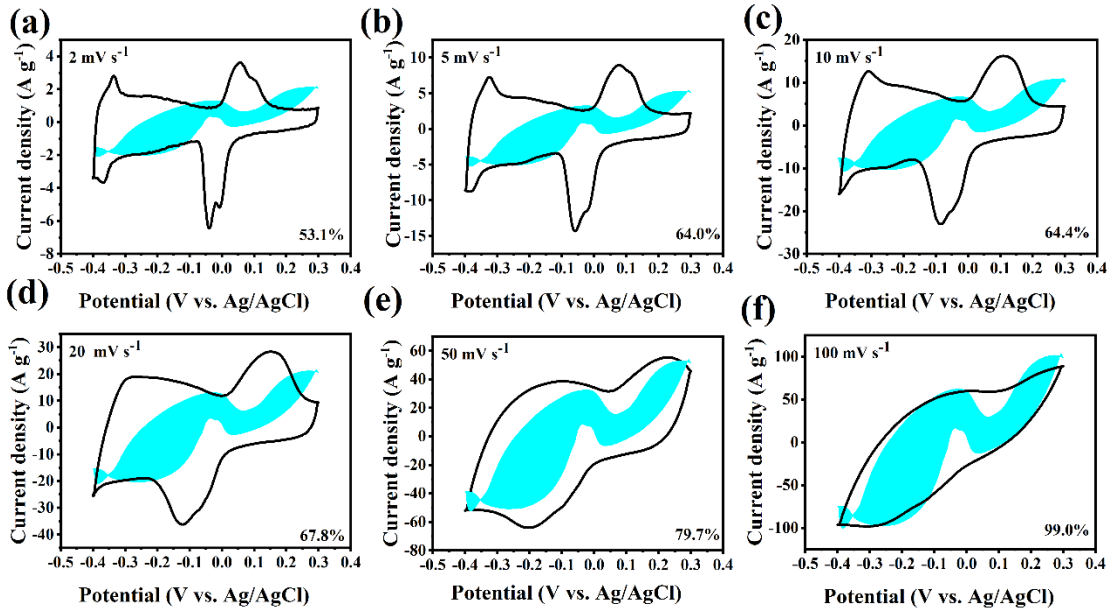

Fig.S7. CV curves of TMP-2 with separation between total currents (black line) and capacitive currents (blue shadow) at (a)2, (b)5, (c) 10, (d) 20, (e) 50 and (f) 100 mV s^{-1}.

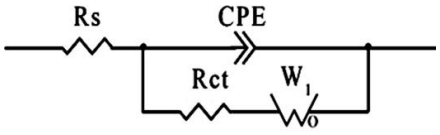

Fig.S8. Nyquist plots of the corresponding equivalent circuit model.

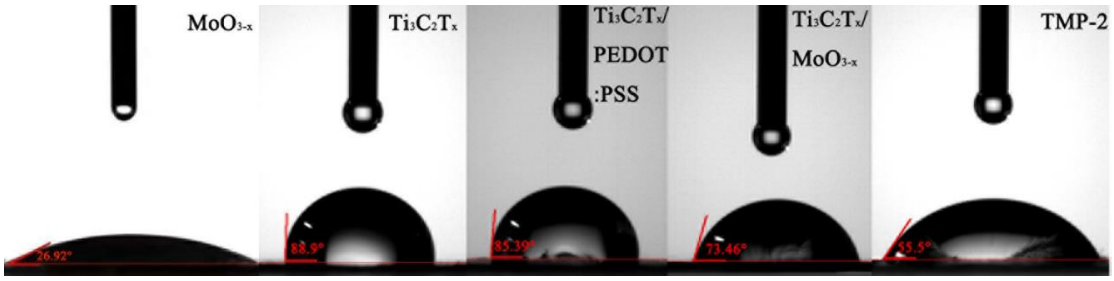

Fig.S9. Water contact angle of samples.

Table S1. Experimental parameters of samples.

Samples	MXene (1.5 mg mL^{-1})	MoO_{3-x}	PEDOT:PSS (1.5 wt%)
$Ti_3C_2T_x$	10 mL	----	----
$Ti_3C_2T_x/MoO_{3-x}$	10 mL	6.42 mg	----
$Ti_3C_2T_x$/PEDOT:PSS	10 mL	----	100 μL
TMP-1	10 mL	3.75 mg	100 μL
TMP-2	10 mL	6.42 mg	100 μL
TMP-3	10 mL	10.00 mg	100 μL

Table S2. Ti 2p XPS spectra fitting results of $Ti_3C_2T_x$ and TMP-2.

Samples	Region	Assigned to	BE [eV]
$Ti_3C_2T_x$	Ti $2p_{3/2}$ ($2p_{1/2}$)	Ti-C	454.9 (460.7)
		Ti^{2+}	455.7 (461.3)
		Ti^{3+}	456.6 (462.2)
		TiO_2	458.6 (463.3)
TMP-2	Ti $2p_{3/2}$ ($2p_{1/2}$)	Ti-C	454.8 (460.7)
		Ti^{2+}	455.7 (461.3)
		Ti^{3+}	456.6 (462.1)
		TiO_2	458.6 (463.3)

Table S3. Mo 3d XPS spectra fitting results of MoO_{3-x} and TMP-2.

Samples	Region	Assigned to	BE [eV]
MoO_{3-x}	Mo $3d_{5/2}$($3d_{3/2}$)	Mo^{6+}	232.7 (235.8)
		Mo^{5+}	231.6 (234.7)
TMP-2	Mo $3d_{5/2}$($3d_{3/2}$)	Mo^{6+}	232.6 (235.8)
		Mo^{5+}	231.6 (234.7)

Table S4. S 2p XPS spectra fitting results of PEDOT:PSS and TMP-2.

Samples	Region	Assigned to	BE [eV]
PEDOT:PSS	S $2P_{3/2}(3d_{1/2})$	PEDOT	163.5 (164.7)
		PSS	167.9 (169.1)
TMP-2	S $3d_{3/2}(3d_{1/2})$	PEDOT	163.6 (164.7)
		PSS	168.0 (169.2)

Table S5. Capacitance performance comparison of MXene-based composites.

Electrode materials	Electrolyte	Gravimatric capacitance	Volumetric capacitance	Ref.
$Ti_3C_2T_x$/RGO	1M H_2SO_4	140 F g^{-1} at 0.5 A g^{-1}	490 F cm^{-3} at 0.5 A g^{-1}	1
Porous MXene/ graphene	3 M H_2SO_4	383 F g^{-1} at 1 A g^{-1}	---	2
PS1MXene	1 M H_2SO_4	506 F g^{-1} at 0.5 A g^{-1}	759 F cm^{-3} at 0.5 A g^{-1}	3
MnO_2/MXene/CC	3 M KOH	511.2 F/g^{-1} at 1 A g^{-1}	----	4
C@Ti_3C_2	6 M KOH	250.6 F g^{-1} at 1 A g^{-1}	---	5
WNRs/MXene	0.5 M H_2SO_4	297 F g^{-1} at 1 A g^{-1}	---	6
MXene-650	1 M H_2SO_4	442 F g^{-1} at 0.5 A g^{-1}	1590 F cm^{-3} at 0.5 A g^{-1}	7
$Ti_3C_2T_x$/BiOCl	1 M KOH	247.8 F g^{-1} at 1 A g^{-1}	396.5 F cm^3 at 1 A g^{-1}	8
i-PANI@$Ti_3C_2T_x$	1 M H_2SO_4	310 F g^{-1} at 1 A g^{-1}	1001 F cm^3 at 1 A g^{-1}	9
$Ti_3C_2T_x$/PANI	3 M H_2SO_4	503 F g^{-1} at 2 mV s^{-1}	1682 F cm^{-3} at 2 mV s^{-1}	10
PPy/$Ti_3C_2T_x$	1 M H_2SO_4	416 F g^{-1} at 5 mV s^{-1}	1000 F cm^{-3} at 5 mV s^{-1}	11
MoO_{3-X}/d-Ti_3C_2	5 M LiCl	---	631 F cm^{-3} at 1 A g^{-1}	12
MXene/ PEDOT:PSS	1 M H_2SO_4	---	1310 F cm^{-3} at 2 mV s^{-1}	13
$Ti_3C_2T_x$/ PEDOT:PSS	1 M H_2SO_4	286 F g^{-1} at 2 mV s^{-1}	1065 F cm^{-3} at 2 mV s^{-1}	14
TMP-2	1 M H_2SO_4	523.0 F g^{-1} at 1A g^{-1}	1898.5 F cm^{-3} at 1A g^{-1}	This work

Table S6. Summary of maximum total capacitance (C_T), double-layer capacitance (C_{dl}) and pseudocapacitance (C_p) for TMP-2 electrodes from the plots of q vs.$v^{1/2}$ and q^{-1} vs. $v^{1/2}$.

C_T	C_{dl}	C_p	C_{dl}/C_T
714.3 F g^{-1}	475.4 F g^{-1}	238.9 F g^{-1}	66.6 %

Table S7. Fitting values of the equivalent circuit elements of samples.

Equivalent circuit elements	**Samples**					
	$Ti_3C_2T_x$	**$Ti_3C_2T_x$/ MoO_{3-x}**	**$Ti_3C_2T_x$ /PEDOT:PSS**	**TMP-1**	**TMP-2**	**TMP-3**
R_s (Ω)	1.403	1.301	1.295	1.237	0.990	1.128
CPE_T	0.00034	0.00020	0.00024	0.00029	0.00038	0.00036
CPE_p	0.92105	1.028	1.027	0.97187	0.97455	0.96985
R_{ct} (Ω)	0.62806	0.4838	0.30346	0.57109	0.48538	0.59812
W_R	1.343	1.659	0.95604	1.002	0.8472	1.091
W_T	0.47173	0.61306	0.46029	0.38657	0.48587	0.50857
W_P	0.48168	0.47268	0.47391	0.47509	0.45841	0.47547

CPE_T is the specific capacitance value when CPE_P=1；

CPE_P is the constant phase element index;

W_R is the diffusion impedance (Warburg diffusion impedance);

W_T is the diffusion time constant;

W_P is the fractional exponent between 0 and 1.

Table S8. The capacitance performance comparison of Mxene-based supercapacitors

Supercapacitors	Electrolyte	Gravimatric capacitance	Volumetric capacitance	Ref.
$Ti_3C_2T_X$@PEDOT// $Ti_3C_2T_X$@PEDOT	1 M H_2SO_4	100 F g^{-1} at 1 A g^{-1}	---	15
d-Ti_3C_2/NF//b-Ti_3C_2	6 M KOH	51.1 F g^{-1} at 0.5 A g^{-1}	---	16
$Ti_3C_2T_x$//rGO/ CNT/PANI	PVA/H_2SO_4 gel	116.9 F g^{-1} at 10 mV s^{-1}	286 F cm^{-3} at 10 mV s^{-1}	17
MnO_2/MXene/CC// MnO_2/MXene/CC	PVA/KOH gel	94.67 F/g^{-1} at 1 A g^{-1}	---	4
C@Ti_3C_2//C@Ti_3C_2	6 M KOH	53.8 F g^{-1} at 1 A g^{-1}	---	5
DMSO-MXene//DMSO-MXene	PVA/KOH gel	74 F g^{-1} at 1 A g^{-1}	---	18
MXene/NCF// MXene/NCF	PVA/KOH gel	63 F g^{-1} at 1 A g^{-1}	519 mF cm^{-3} at 1 A g^{-1}	19
MXene/PEDOT:PSS// MXene/PEDOT:PSS	PVA/H_2SO_4 gel	---	361.4 F cm^{-3} at 2 mV s^{-1}	20
MoO_{3-X}/d-Ti_3C_2//NAC	5 M LiCl	---	79.3 F cm^{-3} at 1 A g^{-1}	12
$Ti_3C_2T_x$/BiOCl// $Ti_3C_2T_x$/BiOCl	1 M KOH	---	64.3 F cm^{-3} at 0.5 A g^{-1}	8
$Ti_3C_2T_x$// PANI@$Ti_3C_2T_x$	3 M H_2SO_4	87.3 F g^{-1} at 10 mV s^{-1}	298.5 F cm^{-3} at 10 mV s^{-1}	21
TMP-2//TMP-2	PVA/H_2SO_4 gel	128.5 F g^{-1} at 1 A g^{-1}	466.4 F cm^{-3} at 1 A g^{-1}	This work

References

1 Y. Zhou, K. Maleski, B. Anasori, J. O. Thostenson, Y. Pang, Y. Feng, K. Zeng, C. B. Parker, S. Zauscher, Y. Gogotsi, J. T. Glass, C. Cao, ACS nano, 2020, **14**, 3576-3586.

2 X. Yang, Q. Wang, K. Zhu, K. Ye, G. Wang, D. Cao, J. Yan, Adv. Funct. Mater., 2021, **31**, 2101087.

3 M. Yao, Y. Chen, Z. Wang, C. Shao, J. Dong, Q. Zhang, L. Zhang, X. Zhao, Chem. Eng. J., 2020, **395**, 124057.

4 H. Zhou, Y. Lu, F. Wu, L. Fang, H. Luo, Y. Zhang, M. Zhou, J. Alloys Compd., 2019, **802**, 259-268.

5 Z. Pan, X. Ji, J. Power Sources, 2019, **439**, 227068.

6 C. Peng, Z. Kuai, T. Zeng, Y. Yu, Z. Li, J. Zuo, S. Chen, S. Pan, L. Li, J. Alloys Compd.,2019, **810**, 151928.

7 X. Zhao, Z. Wang, J. Dong, T. Huang, Q. Zhang, L. Zhang, J. Power Sources, 2020, **470**, 228356.

8 Q. X. Xia, N. M. Shinde, J. M. Yun, T. Zhang, R. S. Mane, S. Mathur, K. H. Kim, Electrochim. Acta, 2018, **271**, 351-360.

9 Y. Zhou, Y. Zou, Z. Peng, C. Yu, W. Zhong, Nanoscale, 2020, **12**, 20797-20810.

10 A. V. Mohammadi, J. Moncada, H. Chen, E. Kayali, J. Orangi, C. A. Carrero, J. Mater. Chem. A, 2018, **6**, 22123-22133.

11 M. Boota, B. Anasori, C. Voigt, M.-Q. Zhao, M. W. Barsoum, Y. Gogotsi, Adv. Mater., 2016, **28**, 1517-1522.

12 W. Zheng, J. Halim, A. S. Etman, A. E. Ghazaly, J. Rosen, M. W. Barsoum, Electrochim. Acta, 2021, **370**, 137665.

13 L. Qin, Q. Tao, A. E. Ghazaly, J. F.-Rodriguez, P. O. Å. Persson, J. Rosen, F. Zhang, Adv. Funct. Mater., 2017, **28**, 1703808.

14 L. Li, N. Zhang, M. Zhang, X. Zhang, Z. Zhang, Dalton Trans., 2019, **48**, 1747-1756.

15 Z. Liu, L. Wanga, Y. Xu, J. Guo, S. Zhang, Y. Lu, J. Electroanal. Chem., 2021, **881**, 114958.

16 J. Guo, Y. Zhao, A. Liu, T. Ma, Electrochim. Acta, 2019, **305**, 164-174.

17 K. Li, X. Wang, X. Wang, M. Liang, V. Nicolosi., Y. Xu, Y. Gogotsi, Nano Energy, 220, **75**, 104971.

18 G. Gao, S. Yang, S. Wang, L. Li, Scripta Materialia, 2022, **213**, 114605.

19 L. Sun, G. Song, Y. Sun, Q. Fu, C. Pan, ACS Appl. Mater. Interfaces, 2020, **12**, 44777-44788.

20 J. Zhang, S. Seyedin, S. Qin, Z. Wang, S. Moradi, F. Yang, P. A. Lynch, W. Yang, J. Liu, X. Wang, J. M. Razal, Small, 2019, **15**, 1804732.

21 K. Li, X. Wang, S. Li, P. Urbankowski, J. Li, Y. Xu, Y. Gogotsi, Small, 2020, **16**, 1906851.